NANO LETTERS

Letter

pubs.acs.org/NanoLett

Revealing Bismuth Oxide Hollow Nanoparticle Formation by the Kirkendall Effect

Kai-Yang Niu,[†] Jungwon Park,[‡] Haimei Zheng,*[,†,‡] and A. Paul Alivisatos*[,†,§]

[†]Materials Sciences Division, Lawrence Berkeley National Laboratory, Berkeley, California 94720, United States

[‡]Department of Materials Science and Engineering, University of California, Berkeley, California 94720, United States

[§]Department of Chemistry, University of California, Berkeley, California 94720, United States

Supporting Information

ABSTRACT: We study the formation of bismuth oxide hollow nanoparticles by the Kirkendall effect using liquid cell transmission electron microscopy (TEM). Rich dynamics of bismuth diffusion through the bismuth oxide shell have been captured in situ. The diffusion coefficient of bismuth through bismuth oxide shell is 3−4 orders of magnitude higher than that of bulk. Observation reveals that defects, temperature, sizes of the particles, and so forth can affect the diffusion of reactive species and modify the kinetics of the hollowing process.

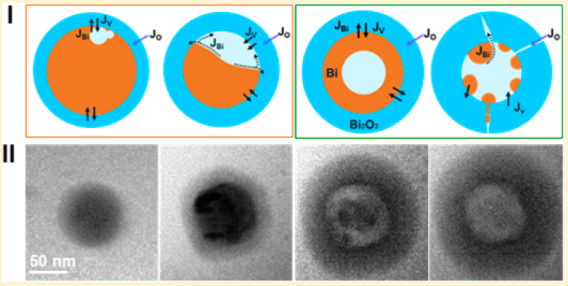

KEYWORDS: *In situ TEM, liquid cell, Kirkendall effect, void formation, diffusion, core−shell nanoparticles*

Synthesis of hollow nanoparticles has been of significant interest due to their distinctive morphology, such as a high surface-to-volume ratio, the void space inside the nanostructure, and high porosity, which enable a variety of applications. For example, there have been studies on using hollow nanoparticles as the carrier for drug delivery,[1] the electrode materials for lithium ion batteries,[2] high sensitive materials for gas sensing,[3,4] and so on. Different methods have been developed to synthesize hollow nanostructures,[5−10] which include using sacrificing templates[2,11] by taking advantage of the Kirkendall effect[5−8] and the galvanic erosion.[12,13] Since the earlier work by Yin et al.,[5] there have been many reports on the colloidal synthesis of hollow nanostructures by Kirkendall effects.[6,7,14−17] During a Kirkendall reaction, the different diffusivities of the atoms in a diffusion couple can induce supersaturation of vacancies at the interface, and the further condensation of excess vacancies and interdiffusion lead to the formation of a hollow nanoparticle. Several growth models have been proposed to elucidate the formation mechanisms of hollow nanoparticles via the Kirkendall effect.[5,6,14,18] For instance, steady-state bulk diffusion has been proposed where the reaction species shuffling through the shell is assumed to be constant and uniformly distributed.[5] Surface-diffusion-mediated growth was also introduced in a number of experiments where a void is formed at the core/shell interface, and further growth of the void is controlled by the diffusion of reactants on the void surface.[8,14] Most of these models are based on ex situ observations. The dynamics of hollowing process is still far from fully understood due to the lack of direct monitoring methods at the nanoscale. Recently, the development of liquid cells for transmission electron microscopy (TEM) allows imaging nanoparticles in liquids with high spatial resolution[19−23] and under heating conditions,[24] which opens the opportunity to elucidate the mechanisms of hollow nanoparticle formation via the Kirkendall effect by real time observation.

In this Letter, we report in situ TEM study of bismuth oxide hollow nanoparticle growth in a liquid cell at an elevated temperature (180−200 °C). A liquid cell consists of two liquid reservoirs and an electron transparent window which allows a thin liquid layer sandwiched between two silicon nitride membranes to be examined (Figure S1).[19,23,24] The liquid precursor was prepared by dissolving 57 mg of Bi 2-ethylhexanoate in a mixture of oleylamine (0.4 mL) and dichlorobenzene (1 mL). About 50 nL of solution was loaded into the cell for in situ TEM experiments. At 180 °C and under electron beam, bismuth nanoparticles nucleate and grow in the solution. Within the time frame of 5−10 min, bismuth nanoparticles grow into 60−80 nm. Subsequently, bismuth nanoparticles are oxidized with a thin bismuth oxide layer on the nanoparticle surface (Figure 1). The oxide layer can be metastable cubic δ-Bi_2O_3 at the initial stage, which can transform into a stable low-temperature phase of monoclinic α-Bi_2O_3. The continuous oxidation of bismuth leads to the formation of a hollow nanoparticle by the Kirkendall effect. In the process of bismuth precursor being reduced to bismuth metal, oleylamine and the electron beam work as reducing reagents in the current reaction conditions.[19] The growth of bismuth metallic nanoparticles follows similar growth trajectories observed in previous publications where coalescence and monomer attachment drive the particle growth.[19,21−24] However, much larger nanoparticles (60−80 nm or larger) have been achieved in this case. And, in the

Received: September 21, 2013
Revised: October 13, 2013
Published: October 16, 2013

ACS Publications © 2013 American Chemical Society

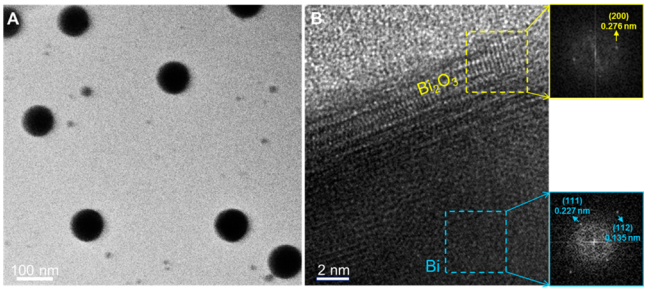

Figure 1. (A) Bright field TEM image of bismuth nanoparticles formed inside a liquid cell. (B) High-resolution TEM image of an as-formed Bi nanoparticle. The surface of Bi nanoparticles is oxidized in a short time at 180 °C.

subsequent process of hollow nanoparticle formation, we have observed rich diffusion dynamics of bismuth and the growth kinetics of bismuth oxide governed by the Kirkendall effect.

Figure 2 shows a few image series of bismuth oxide hollow nanoparticle formation with different morphology evolution. In Figure 2A–C (particle I), a thin layer of bismuth oxide is formed on the surface of the nanoparticle at the early stage. Subsequently, voids start to develop at the core/shell interface as indicated by the distinct contrast difference within the oxide shell. As the thickness of bismuth oxide shell increases, the void becomes bigger by consuming bismuth. The bismuth core starts disappearing in layer-by-layer fashion, and the interface morphology changes dynamically (also see Movies S1–S2). Eventually, a nonuniform shell is formed with thicker shell close the void as shown in Figure 2B (also see details of the thickness evolution in Figure S2). It indicates that bismuth diffuses out of the oxide shell nonuniformly with the faster diffusion through the shell adjacent to the void. We measured the diffusion rate of bismuth through the shell by calculating the volume of the shell as a function of time. The results are plotted in Figure 2C. The diffusion coefficient of bismuth in the bismuth oxide shell can be estimated using Fick's law. The diffusion flux of bismuth in the oxide shell is approximately $J = D(\rho - 0)/\bar{d}$, where D is the diffusion coefficient, ρ is the density of bismuth oxide, and $\bar{d}$ is the average oxide shell thickness. The diffusion cross section can be

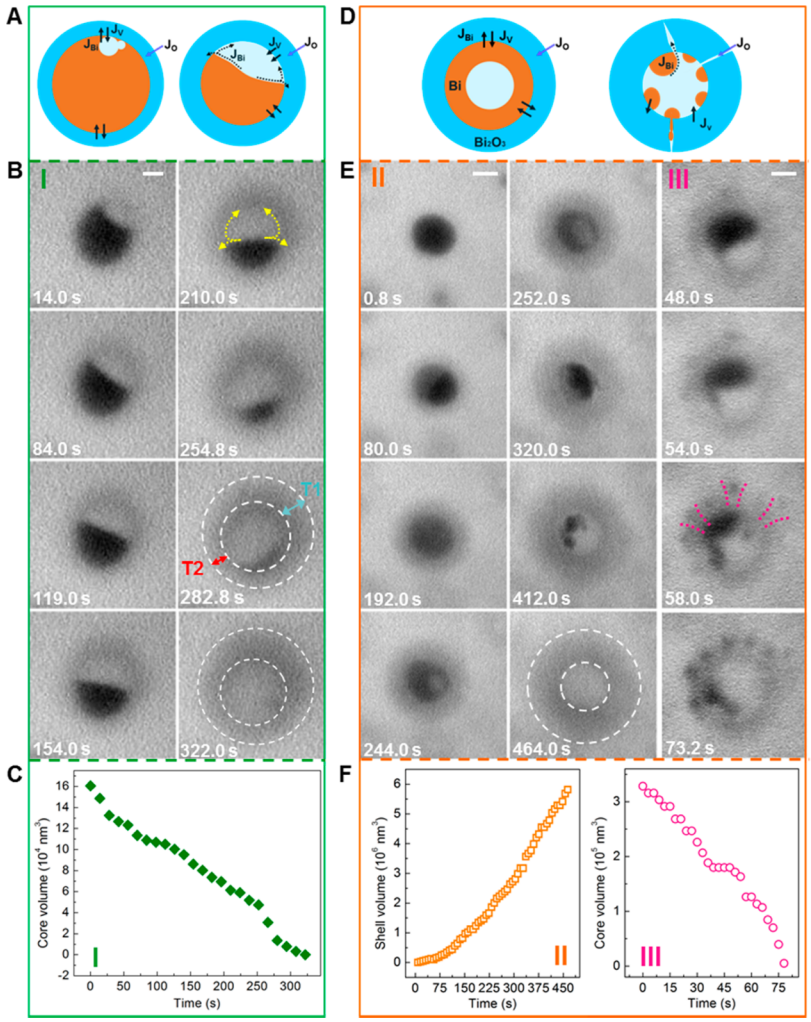

Figure 2. Hollow nanoparticle growth dynamics via Kirkendall effects. (A) A schematic diagram of the evolution mechanisms of hollow nanoparticles dominated by nonuniform diffusion of bismuth through void surfaces (Movies S1 and S2). (B) TEM image series of the formation of hollow nanoparticles (Movie S1); the scale bar is 20 nm. (C) Volume change of the core of particle I shown in B. (D) Schematic diagram of the evolution mechanism of hollow nanoparticles dominated by diffusion of bismuth directly through the shell (Movies S3–S7). (E) Snapshots of the hollow particle evolution of particle II (Movie 2S) and particle III (Movie S7); the scale bars are 50 nm. (F) Shell volume of particle II and core volume of particle III as a function of time as shown in E.

dx.doi.org/10.1021/nl4035362 | *Nano Lett.* 2013, 13, 5715–5719

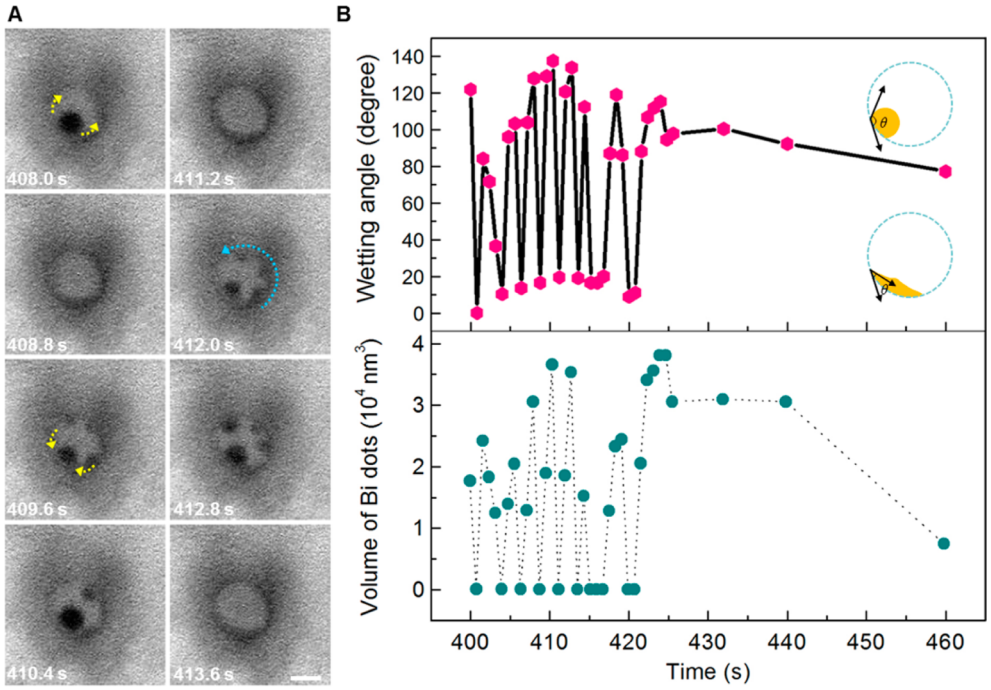

Figure 3. Dynamics of the residue bismuth at the later stage of hollow nanoparticle formation. (A) Sequential images show bismuth behaves like liquids with frequent changes of configuration; the scale bar is 50 nm. (B) Oscillation of the average wetting angle of the bismuth nanodots shown in A. Wetting angle is measured by the angle between the tangent of bismuth oxide shell and that of a bismuth nanoparticle inside. (D) Volume change of Bi in A calculated from two-dimensional projections; the volume under complete wetting conditions counts as 0.

approximated as the inner surface area of the shell, that is, $S = 4\pi r^2$ where r is the inner radius of the shell. The time $t_{1/2}$ for bismuth in the core decreases to half of its initial volume can be expressed as:

$$t_{1/2} = \frac{(1/2) \times (4/3)\pi r^3 \rho}{JS} = \frac{(1/2) \times (4/3)\pi r^3 \rho}{(D\rho/\bar{d}) \times 4\pi r^2} = \frac{1}{6} \times \frac{r\bar{d}}{D} \quad (1)$$

From Figure 2C, $t_{1/2}$ for particle I is about 168 s. Therefore, the average diffusion coefficient of particle I is $D_I = 0.75$ nm^2/s $= 0.75 \times 10^{-14}$ cm^2/s, which is about 3 orders of magnitude larger than the bulk self-diffusion coefficient of Bi in Bi_2O_3: $D \approx 10^{-17}$ cm^2/s at 180 °C.[25]

Figure 2E shows sequential images of the formation of two other bismuth oxide hollow nanoparticles, particle II and particle III, following different pathways (also see Movie S3). At the early stage (the first 215 s), a bismuth oxide shell is formed on the surface of the bismuth nanoparticle, and there are subtle contrast changes in the bismuth core, indicating bismuth diffuses out of the particle and gets oxidized. The contrast changes within the bismuth core gradually become obvious, which suggests randomly distributed smaller voids/vacancies condense into larger voids inside the core. At the end, the small amount of residue bismuth becomes unstable and behaves like liquids. It can suddenly split into several nanodroplets and then vanish quickly. The frequent changes of the bismuth configuration suggest the local temperature is over the melting point of residual bismuth. The melting temperature of nanoparticles decreases at the nanoscale.[26,27] For instance, the melting temperature of the 10 nm bismuth nanoparticle is about 180 °C, which is significantly lower than that for bulk bismuth (i.e., 271 °C).[28] It is not surprising that the residue bismuth behaves like liquid rather than solid when it becomes less than tens of nanometers. We measured the volume increases of bismuth oxide shell as a function of time, and the results are plotted in Figure 2F(II). Here, the shell thickness increase instead of bismuth core loss is used because there are multiple contrast changes in the bismuth core which make it hard to evaluate the core mass accurately. Bismuth diffusion through the shell can be estimated by assuming all of the bismuth diffuses out of the shell to form the bismuth oxide shell. The time $t_{1/2}$ for the half volume change of bismuth core is the same as that for bismuth oxide shell. The diffusion coefficient (D_{II}) of bismuth through the bismuth oxide shell can be calculated using eq 1, and $D_{II} = 1.88 \times 10^{-14}$ cm^2/s is achieved.

We further found that some nanoparticles show the formation of clusters on the outer surface of the particle (Figure 2E(III)). It is likely that defects in the shell such as grain boundaries serve as diffusion channels,[14,29] which facilitates the outward diffusion of the core species. Bismuth tends to condense into nanoparticles before they get oxidized. Due to the existence of the various diffusion channels, the rate of shell growth can be enhanced (Figure 2F(III)). A diffusion coefficient of bismuth in the bismuth oxide shell, $D_{III} = 7.56 \times 10^{-14}$ cm^2/s, is obtained from eq 1.

The different scenarios of hollow nanoparticle formation are summarized in Figure 2A and D. A void can be developed either at the core/shell interface or condense inside the particle from the excessive vacancies. Approximately, the diffusion coefficient of bismuth through the bismuth oxide shell is 3−4 orders of magnitude higher than that of bulk. There could be multiple diffusion pathways, including surface-mediated diffusion, uniform diffusion through the shell, and so forth. Defects in the shell can act as diffusion channels to facilitate the outward diffusion of bismuth. Slightly different diffusion rates associated with various

dx.doi.org/10.1021/nl4035362 | Nano Lett. 2013, 13, 5715−5719

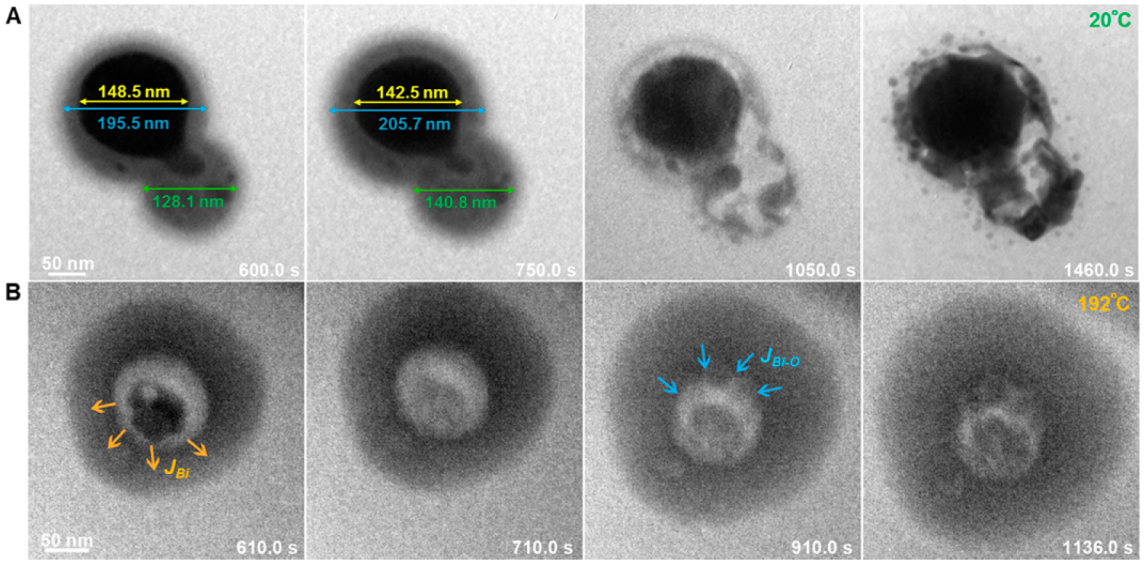

Figure 4. (A) Kirkendall effects occurred at room temperature; the starting point is set arbitrarily. (B) A bismuth oxide hollow nanoparticle formed at 190 °C and its collapse by inward mass diffusion.

diffusion pathways have been observed (see the above values of D_{I}, D_{II}, and D_{III}).

Figure 3A shows bismuth liquid nanodroplets inside the bismuth oxide shell, which display a reversible wetting transition on the curved inner surface of the shell. The liquid droplets can completely wet the inner surface of the bismuth oxide. Then, since such a configuration is not stable, it splits into several dewetting nanodropets instantaneously. These nanodroplets can aggregate or migrate on the curved inner surface before liquid bismuth completely wets the inner surface again (Movie S3). The reversible wetting transitions repeated 8 times within 20 s, and the total volume of the core species calculated from the two-dimensional projection fluctuates (Figure 3B). There is no significant bismuth mass loss during the fluctuations. We consider the wetting transition can be attributed to the interplay between the surface tension of liquid bismuth and the surface properties of bismuth oxide shell. Variation in the vapor pressure inside the shell, temperature, diffusion of bismuth on the curved surface, and so forth can contribute to the fluctuations in its wetting behavior.

Surface diffusion plays a critical role in the evolution of hollow nanoparticles via the Kirkendall effect.[8] The observed different growth modes indicate that the differences in diffusivity of the two elements (Bi and O in Bi_2O_3) is not the only impact factor for the formation of Kirkendall-type hollow nanoparticles, and other factors may play a role, for instance, the collision frequency of oxidative radicals with the bismuth nanoparticle surface, the probability for the surrounding oxidative radicals to be trapped, the probability for the oxidative species to reach the Bi/Bi_2O_3 interface and the Bi atoms/ions to reach the Bi_2O_3/solution interface, and so forth.[14,15,18] All of these above are dependent on the temperature, solution viscosity, concentration of the oxidants, and size of the Bi nanoparticles. Thus, the hollow nanoparticle reaction kinetics is complex.

Temperature can drastically affect the Kirkendall reaction by modifying the diffusion rate, activation energy, and stability of the voids. We have investigated the evolution of hollow nanoparticles at different temperatures. At room temperature, nanoparticles can be slowly oxidized with no obvious voids (Figure 4A). Under such low-temperature growth conditions, the reaction probabilities can be low, and they can be comparable at both Bi/Bi_2O_3 and Bi_2O_3/solution interfaces. As a result, the ions could diffuse homogeneously cross the shell (marked by arrows in Figure 4A); the shell species could grow on both inner and outer surfaces of shell, and a solid oxide particle is produced. We suspect that only amorphous bismuth oxide can be achieved, but more experiments are needed for identifying the structure. The continuous electron beam irradiation can damage the shell, where the bismuth oxide can be reduced as indicated by the clusters on the particle surface at the later stage. At higher temperature, that is, 192 °C, a perfect hollow particle is formed (Figure 4S). However, the hollow nanoparticle is not stable, that the void is gradually filled (Figure 4B).

It has been elaborated previously that hollow nanoparticles could shrink via outward diffusion of vacancy flux under a thermodynamically controlled condition and the driving force is the difference in the chemical potential of vacancies on the inner and external surface of the shell (i.e., the Gibbs−Thomson effect). Considering a hollow particle with inner shell radius r_1 and outer radius r_2, we can get the vacancy concentration near the inner and outer surfaces from the Gibbs−Thomson equation:[30−32]

$$C_{\mathrm{v}}^{1} = C_{\mathrm{v}}^{0} \exp\left(\frac{2\lambda\Omega}{kTr_1}\right) \tag{2}$$

$$C_{\mathrm{v}}^{2} = C_{\mathrm{v}}^{0} \exp\left(\frac{2\lambda\Omega}{kTr_2}\right) \tag{3}$$

where C_{v}^{1}, C_{v}^{2}, and C_{v}^{0} are the vacancy concentrations near the inner surface, outer surface of the hollow particle, and near the reference planar surface in a bulk sample, respectively; and λ is the surface energy per unit area, Ω is the atomic volume of a vacancy. There is a vacancy concentration gradient from the inner surface to the outer surface of the shell, $C_1 > C_0 > C_2$, across the hollow shell, which provides a driving force for the outward diffusion of the vacancy flux. Also, the excessive heat input enhances the interdiffusion processes. In addition, the diffusion of oxygen in the as-formed Bi_2O_3 can be enhanced due to the

dx.doi.org/10.1021/nl4035362 | Nano Lett. 2013, 13, 5715−5719

electron beam.[33] Therefore, the void in the hollow particle could be filled at higher temperatures.

In conclusion, we have studied the formation of bismuth oxide hollow nanoparticles under temperature-controlled growth condition using liquid cell TEM. Different diffusion pathways of bismuth through the bismuth oxide shell, kinetics, and the factors that affect the Kirkendall hollowing process have been identified and discussed. An understanding of mechanisms of hollow nanoparticle formation at a single particle level may assist the future design of materials with desired functions. Beyond studying hollow nanoparticle formation we introduced here, liquid cell TEM with temperature control provides an opportunity to investigate many other chemical reactions under controlled reaction conditions at the nanometer length scale.

■ ASSOCIATED CONTENT

Supporting Information

A description of materials and methods, Figures S1−S5, and seven supporting movies. This material is available free of charge via the Internet at http://pubs.acs.org.

■ AUTHOR INFORMATION

Corresponding Authors

*E-mail: hmzheng@lbl.gov.
*E-mail: alivis@berkeley.edu.

Present Address

J.P.: School of Engineering and Applied Sciences, Harvard University, Cambridge, Massachusetts 02138, United States.

Notes

The authors declare no competing financial interest.

■ ACKNOWLEDGMENTS

The experiments were conducted using both MSD TEM facility and a JEOL3010 microscope at National Center for Electron Microscopy (NCEM) of the Lawrence Berkeley National Laboratory (LBNL), which is supported by the U.S. Department of Energy (DOE) under contract no. DE-AC02-05CH11231. H.Z. thanks the DOE Office of Science Early Career Research Program for their support.

■ REFERENCES

(1) Shin, J.; Anisur, R. M.; Ko, M. K.; Im, G. H.; Lee, J. H.; Lee, I. S. *Angew. Chem., Int. Ed.* **2009**, *48* (2), 321−324.
(2) Lou, X. W.; Wang, Y.; Yuan, C.; Lee, J. Y.; Archer, L. A. *Adv. Mater.* **2006**, *18* (17), 2325−2329.
(3) Zhao, Q.; Gao, Y.; Bai, X.; Wu, C.; Xie, Y. *Eur. J. Inorg. Chem.* **2006**, *2006* (8), 1643−1648.
(4) Niu, K. Y.; Yang, J.; Kulinich, S. A.; Sun, J.; Du, X. W. *Langmuir* **2010**, *26* (22), 16652−16657.
(5) Yin, Y.; Rioux, R. M.; Erdonmez, C. K.; Hughes, S.; Somorjai, G. A.; Alivisatos, A. P. *Science* **2004**, *304* (5671), 711−714.
(6) Wang, W.; Dahl, M.; Yin, Y. *Chem. Mater.* **2012**, *25* (8), 1179−1189.
(7) Peng, S.; Sun, S. *Angew. Chem.* **2007**, *119* (22), 4233−4236.
(8) Fan, H. J.; Knez, M.; Scholz, R.; Hesse, D.; Nielsch, K.; Zacharias, M.; Gösele, U. *Nano Lett.* **2007**, *7* (4), 993−997.
(9) Niu, K. Y.; Yang, J.; Kulinich, S. A.; Sun, J.; Li, H.; Du, X. W. *J. Am. Chem. Soc.* **2010**, *132* (28), 9814−9819.
(10) Niu, K.-Y.; Yang, J.; Sun, J.; Du, X.-W. *Nanotechnology* **2010**, *21*, 295604.
(11) Khanal, A.; Inoue, Y.; Yada, M.; Nakashima, K. *J. Am. Chem. Soc.* **2007**, *129* (6), 1534−1535.
(12) Sun, Y.; Mayers, B.; Xia, Y. *Adv. Mater.* **2003**, *15* (7−8), 641−646.
(13) González, E.; Arbiol, J.; Puntes, V. F. *Science* **2011**, *334* (6061), 1377−1380.
(14) Fan, H. J.; Goesele, U.; Zacharias, M. *Small* **2007**, *3* (10), 1660−1671.
(15) Cabot, A.; Ibáñez, M.; Guardia, P.; Alivisatos, A. P. *J. Am. Chem. Soc.* **2009**, *131* (32), 11326−11328.
(16) Chiang, R.-K.; Chiang, R.-T. *Inorg. Chem.* **2007**, *46* (2), 369−371.
(17) Knez, M.; Scholz, R.; Nielsch, K.; Pippel, E.; Hesse, D.; Zacharias, M.; Gösele, U. *Nat. Mater.* **2006**, *5* (8), 627−631.
(18) Ibáñez, M.; Fan, J.; Li, W.; Cadavid, D.; Nafria, R.; Carrete, A.; Cabot, A. *Chem. Mater.* **2011**, *23* (12), 3095−3104.
(19) Zheng, H.; Smith, R. K.; Jun, Y.-w.; Kisielowski, C.; Dahmen, U.; Alivisatos, A. P. *Science* **2009**, *324* (5932), 1309−1312.
(20) de Jonge, N.; Ross, F. M. *Nat. Nanotechnol.* **2011**, *6* (11), 695−704.
(21) Yuk, J. M.; Park, J.; Ercius, P.; Kim, K.; Hellebusch, D. J.; Crommie, M. F.; Lee, J. Y.; Zettl, A.; Alivisatos, A. P. *Science* **2012**, *336* (6077), 61−64.
(22) Evans, J. E.; Jungjohann, K. L.; Browning, N. D.; Arslan, I. *Nano Lett.* **2011**, *11* (7), 2809−2813.
(23) Liao, H.-G.; Cui, L.; Whitelam, S.; Zheng, H. *Science* **2012**, *336* (6084), 1011−1014.
(24) Xin, H. L.; Zheng, H. *Nano Lett.* **2012**, *12* (3), 1470−1474.
(25) Palkar, G. D.; Sitharamarao, D. N.; Dasgupta, A. K. *Trans. Faraday Soc.* **1963**, *59* (0), 2634−2638.
(26) Ohashi, T.; Kuroda, K.; Saka, H. *Philos. Mag., Part B* **1992**, *65* (5), 1041−1052.
(27) Qi, W. H.; Wang, M. P. *Mater. Chem. Phys.* **2004**, *88* (2−3), 280−284.
(28) Allen, G. L.; Bayles, R. A.; Gile, W. W.; Jesser, W. A. *Thin Solid Films* **1986**, *144* (2), 297−308.
(29) Aidhy, D. S.; Nino, J. C.; Sinnott, S. B.; Wachsman, E. D.; Phillpot, S. R. *J. Am. Ceram. Soc.* **2008**, *91* (7), 2349−2356.
(30) Evteev, A. V.; Levchenko, E. V.; Belova, I. V.; Murch, G. E. *Philos. Mag.* **2008**, *88* (10), 1525−1541.
(31) Evteev, A. V.; Levchenko, E. V.; Belova, I. V.; Murch, G. E. *Philos. Mag.* **2007**, *87* (25), 3787−3796.
(32) Gusak, A. M.; Zaporozhets, T. V.; Tu, K. N.; Gosele, U. *Philos. Mag.* **2005**, *85* (36), 4445−4464.
(33) Aidhy, D. S.; Sinnott, S. B.; Wachsman, E. D.; Phillpot, S. R. *Ionics* **2010**, *16* (4), 297−303.